

Nano-optical Investigations of the Metal–Insulator Phase Behavior of Individual VO₂ Microcrystals

Andrew C. Jones,^{†,‡} Samuel Berweger,[‡] Jiang Wei,[†] David Cobden,[†] and Markus B. Raschke^{*,†,‡}

[†]Department of Physics and [‡]Department of Chemistry, University of Washington, Seattle, Washington 98195

ABSTRACT Despite the relatively simple stoichiometry and structure of VO₂, many questions regarding the nature of its famous metal–insulator transition (MIT) remain unresolved. This is in part due to the prevailing use of polycrystalline film samples and the limited spatial resolution in most studies, hindering access to and control of the complex phase behavior and its inevitable spatial inhomogeneities. Here, we investigate the MIT and associated nanodomain formation in individual VO₂ microcrystals subject to substrate stress. We employ symmetry-selective polarization Raman spectroscopy to identify crystals that are strain-stabilized in either the monoclinic M1 or M2 insulating phase at room-temperature. Raman measurements are further used to characterize the phase dependence on temperature, identifying the appearance of the M2 phase during the MIT. The associated formation and spatial evolution of rutile (R) metallic domains is studied with nanometer-scale spatial resolution using infrared scattering-scanning near-field optical microscopy (s-SNOM). We deduce that even for small crystals of VO₂, the MIT is influenced by the competition between the R, M1, and M2 crystal phases with their different lattice constants subjected to the external substrate-induced stress. The results have important implications for the interpretation of the investigations of conventional polycrystalline thin films where the mutual interaction of constituent crystallites may affect the nature of the MIT in VO₂.

KEYWORDS Vanadium dioxide, metal-to-insulator transition, near-field microscopy, Raman spectroscopy

A number of transition metal oxides exhibit metal–insulator transitions (MIT) that can be induced by temperature, stress, and/or doping.^{1,2} One of the most widely studied, because of its potential applications, is vanadium dioxide (VO₂), which undergoes a first-order MIT from a low-temperature monoclinic insulating phase to a high-temperature rutile (R) metallic phase at $T_{\text{MIT}} = 340$ K.¹ Despite its early discovery, convenient transition temperature, and comparatively simple crystal structure, the underlying mechanism behind the MIT in VO₂ is still debated as the transition exhibits both Peierls-like and Mott-like characteristics.^{2–8}

Involving both electronic and lattice degrees of freedom, the MIT in VO₂ has been shown to be affected by doping⁹ as well as stress.^{10,11} Furthermore, VO₂ exhibits more than one low-temperature insulating crystallographic structure, the primary ones being the monoclinic M1 (low stress/low Cr doping) and M2 (high stress/high Cr doping) phases.^{9,10,12,13} Although the M2 phase has previously received little experimental attention, the fact that its crystal structure can be viewed as intermediate between M1 and R¹⁴ suggests that the study of its properties may be key in understanding the MIT.^{8,14} Recent studies have identified the M2 phase via X-ray diffraction

in ensembles of VO₂ single crystals¹¹ and via Raman spectroscopy in single surface bound/clamped crystals.¹⁵ However, details of the nanoscale domain formation and phase behavior of the M1, M2, and R phases, together with their complex dependence on stress and temperature are not yet fully understood.

Because of changes in the lattice parameters associated with this displacive MIT, bulk crystals suffer from strain-induced degradation in repeated cycling across T_{MIT} .¹⁶ For related reasons, the MIT in polycrystalline VO₂ thin films is broadened over a wider temperature range^{17–19} than in single crystals¹ as a result of a highly inhomogeneous macroscopic material response^{20,21} possibly the result of inevitable nonuniform local stress. This makes the interpretation of macroscopic measurements on polycrystalline samples difficult and calls for investigations of the properties of individual single crystals. The study of individual small VO₂ single crystals avoids averaging over an inhomogeneous ensemble¹¹ and eliminates the granular structure of polycrystalline films^{20,21} providing access to the correlation of the MIT with intrinsic crystallographic properties as well as the influence of stress.

Here, we investigate the MIT of small individual VO₂ crystals bound to an oxidized Si substrate. These micrometer-sized crystals are highly resistant to degradation on thermal cycling.^{22–24} It has previously been shown that the substrate-induced stress from the elastic misfit in the fused crystal/substrate system results in the formation of periodic metallic

*To whom correspondence should be addressed. E-mail: raschke@chem.washington.edu.

Received for review: 11/10/2009

Published on Web: 04/08/2010



and insulating domains during the MIT.^{22,23} The study of this system should provide important information relevant for the interpretation of measurements on disordered polycrystalline films.

We use a combination of two purely optical techniques that stand out for their experimental simplicity, minimal interference with the intrinsic phase behavior, and lack of need for special sample preparation. Infrared (IR) scattering-scanning near-field optical microscopy (*s*-SNOM) provides dielectric contrast and spatial resolution²⁵ to access the nanometer spatial evolution of insulating and metallic domains as demonstrated previously for polycrystalline films.²⁰ The particular combination of far-field Raman microscopy and *s*-SNOM provides identification of the M1 and M2 insulating phases of individual crystals and allows monitoring of the nanoscale spatial evolution of ordered insulating and metallic domains during the MIT process.

We observe that all VO₂ crystals for a given sample are stabilized in either the M1 or M2 insulating phase at ambient temperature, which appears to be a consequence of different strain related to variations in growth conditions. Insulating domains in crystals initially in the M1 phase at room temperature are found to convert to the M2 phase during the MIT prior to the formation of the fully metallic state. Crystals initially in the M2 phase convert directly via the formation and growth of periodic R domains in a similar fashion but at slightly higher temperatures compared to the M1 case. Associated with the M2 phase we observe a subdomain striation within the insulating M2 regions on length scales of ~100 nm recently identified to be due to polysynthetic twinning.²⁶

It is known that the M2 phase, which in the unstrained material has a free energy very close to that of M1, can be stabilized by doping or compressive uniaxial stress in the [110]_R direction.^{9,10} The relationship between the crystal lattices of the different phases of VO₂ can be understood in terms of the displacement and pairing of two interpenetrating sublattices, A and B, each composed of chains of V atoms oriented along the crystallographic *c_R* axis. In the rutile phase, each V atom is octahedrally coordinated with oxygen with the octahedral axis pointing along the [110]_R (A) or [1 $\bar{1}$ 0]_R (B) direction (see schematic R in Figure 1c).^{9,10} From the R crystal structure, the M2 insulating phase is formed through the differentiation of the two V sublattices. For sublattice A, V atoms dimerize in rows approximately along the *c_R* direction, while in sublattice B the pairwise tilt of V atoms leads to the formation of a zigzag chain along the approximate *c_R* axis (see schematic M2). In M1 all V pairs are both dimerized and tilted (see schematic M1).²⁷

In addition to changes in the crystal lattice symmetry associated with the tilting/dimerization of the V atoms, the lattice constants differ between the M1, M2, and R phases. The lattice constants of the M1 phase as compared to R are shorter by ~0.6% along the *a_R* axis, shorter by ~0.4% along the *b_R* axis, and longer by ~1.0% along the *c_R* axis.^{28,29} The

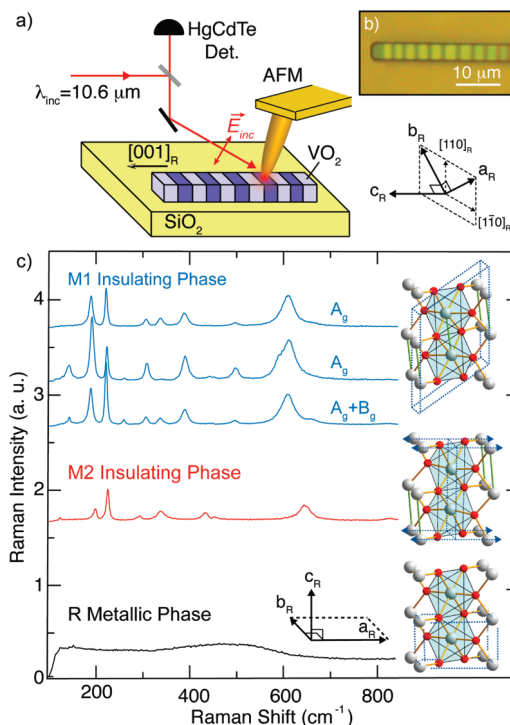


FIGURE 1. Schematic of the IR *s*-SNOM experiment (a) for characterization of domain formation of substrate bound VO₂ crystals (b). Raman spectra from freestanding VO₂ crystals (c) with lattice representations of the M1, M2, and R crystal structures centered around oxygen octahedra oriented along the [110]_R direction. The three Raman spectra for the M1 phase (top to bottom) were taken for illumination/detection polarization with respect to the longitudinal (*c_R*) axis of the crystal of parallel/parallel, perpendicular/perpendicular, and parallel/unpolarized yielding the A_g modes for the first two cases and a superposition of the A_g and B_g modes for unpolarized detection.

lattice constants of the M2 phase as compared to R are shorter by ~0.4% along the *a_R* axis, shorter by ~0.7% along the *b_R* axis, and longer by ~1.7% along the *c_R* axis.^{9,28,29} The resulting volume changes from the R to the M1 and M2 insulating phases are -0.044²⁹ and 0.6%,⁹ respectively.

Experiment. The VO₂ crystals are grown by vapor phase transport as described previously.^{22,30} VO₂ (Sigma-Aldrich, ≥ 99.99%) powder placed upstream from an oxidized silicon substrate is heated to ~1275 K in a tube furnace with 20 mbar of argon carrier gas for 30 min. The resulting single crystals that grow on the substrate have roughly rectangular cross sections with thickness in the range of 25–200 nm, widths between 50 nm and several micrometers, and lengths up to hundreds of micrometers. As known from X-ray diffraction³⁰ and confirmed by our Raman measurements, the longitudinal axis corresponds to the [100]_{M1} = [001]_R crystallographic *c*-axis direction of the metallic R phase.

The formation of micrometer-scale alternating metallic and insulating domains in these surface-adhered crystals, as readily observed by far-field microscopy, involves the interplay of the mismatch of the thermal expansion coefficients between VO₂ and the substrate, the crystal volume change associated with the MIT, the free energies of the respective

phases, and the energy associated with domain wall formation.^{22,31} At temperatures above T_{MIT} the crystals experience tensile stress due to the higher thermal expansion coefficient of VO_2 compared with the Si/SiO_2 substrate. This stress is expected to be larger along the long axis of the crystal (c_{R} axis) due to the larger thermal expansion coefficient in the c_{R} direction.²⁹ This promotes the appearance of insulating domains at temperatures above T_{MIT} , whose formation reduces the average stress along the crystal as their lattice constants are larger in the c_{R} direction compared to the R phase. On cooling these domains grow until the metallic phase has completely disappeared, at which point the axial stress has become compressive (see Discussion below). Crystals released from the substrate exhibit no domain formation converting entirely to the insulating or metallic phase near T_{MIT} .

Raman scattering experiments as used for phase identification are performed using a home-built micro-Raman setup in an epi-illumination and detection geometry using a $\text{NA} = 0.75$ objective (Olympus, $50\times$). For illumination, we use a continuous wave HeNe laser ($\lambda = 632.8$ nm) with incident power of <0.01 mW to minimize sample heating. The scattered light is filtered with a long-pass filter with a cutoff corresponding to a Raman shift of ~ 160 cm^{-1} and detected with an imaging spectrograph with a $\text{N}_2(\text{l})$ -cooled CCD (Acton Research).

The IR *s*-SNOM experimental setup, as shown schematically in Figure 1a, is based on a modified atomic force microscope (AFM, CP-Research, Veeco Inc.). A CO_2 laser with wavelength $\lambda \approx 10.6$ μm is focused onto a Pt-coated AFM probe (Nanosensors, ATEC) with a Cassegrain objective ($\text{NA} = 0.5$) at an angle of 65° with respect to the surface normal (elliptical focus size of ≈ 30 μm in width, incident power ≈ 5 mW). The incident polarization is primarily oriented parallel with respect to the tip axis (Figure 1a). The tip-scattered near-field response is detected by a mercury–cadmium–telluride (MCT) detector (Kolmar, Model KLD-0.25/DC/11.5) and discriminated against the far-field background via lock-in detection on the second-harmonic of the cantilever dither oscillation frequency.^{25,32}

Optical excitation in the 6–12 μm mid-IR range, that is, well above the optical phonon energies and below the interband transition, allows for optimal contrast between the insulating and metallic phases of the VO_2 .^{33,34} The image contrast due to the optical dipole–dipole coupling between tip and sample is determined by the local spatially varying dielectric function of the surface. Regions of the metallic phase, with comparatively large IR optical conductivity, provide a higher effective tip–sample polarizability and thus a higher IR-*s*-SNOM signal compared to the dielectric insulating phases.^{25,35,36} The typically observed *s*-SNOM spatial resolution of 10–20 nm is conventionally determined by the radius of curvature of the AFM tip.²⁵

Results. Figure 1c shows room temperature Raman spectra identifying free-standing VO_2 crystals protruding

from the edge of the substrate wafer to be in the M1 and M2 insulating phases.^{37–41} We were able to obtain the M2 phase for certain freestanding crystals, induced as a metastable state by the micrometer-size laser focus using slightly higher illumination intensities.⁴²

The space groups for the R, M1, and M2 lattices are D_{4h}^{14} , C_{2h}^3 , and C_{2h}^5 , respectively.²⁸ The M1 phase is thus characterized by 18 Raman active modes with $9A_g$ and $9B_g$ modes.⁴³ The M2 phase also exhibits 18 Raman active modes with a slightly different distribution with $10A_g$ and $8B_g$ modes.⁴⁰ The M1 and M2 Raman spectra differ primarily in shifts of the 607 and 189 cm^{-1} M1 phonon frequencies to higher energies, the decrease of the 441 cm^{-1} mode frequency, and the splitting of the 221 cm^{-1} M1 mode. This, together with the spectrum of the R phase which is dominated by a featureless luminescence,^{37,38} allows for the unambiguous distinction between the M1, M2, and R phases.

Our Raman room temperature measurements of individual crystals bound to the substrate identify every crystal in a given macroscopic sample region as being either fully in the M1 or M2 insulating phase, that is, no mixture of M1 and M2 crystals was found. The mechanism of the stabilization of the M1 and M2 phases at room temperature will be discussed below. Crystals in M2 at room temperature were found to relax into the M1 phase after loosening from the surface by a buffered-oxide etch. This is indicative of the dominant role of stress in the phase behavior, although additional factors such as oxygen deficiency from the growth process cannot be completely ruled out.

Figure 2 shows topography (panel d) and simultaneously recorded *s*-SNOM data (panels a–c) following a VO_2 crystal initially in the M1 phase at room-temperature through the MIT. Such crystals convert from the low-temperature fully insulating state (panel a) through the sudden appearance of a first metallic domain (panels b and f, 341 K), to a roughly periodic set of insulating and metallic domains (c and f, 345 K), to the fully metallic state at temperatures of 370–390 K (*s*-SNOM data not shown).

The initial appearance of metallic domains is reflected in the Raman spectra by a sharp rise in the luminescence background (Figure 2g, arrow). Up to ~ 350 K the insulating domains of the regular domain pattern formed remain purely M1 phase. As the temperature is increased further and the insulating domains begin to shrink in size a conversion of M1 to M2 is observed as seen from the appearance of the characteristic M2 Raman modes (Figure 2g, 351 K spectrum). Within a narrow temperature range of ~ 5 K all insulating domains convert to M2 (Figure 2g, 355 K) without a significant change in the total fraction of R. This M1 \rightarrow M2 conversion occurs around 30 K below the temperature where the fully metallic state is reached.

Figure 2f shows the associated domain formation and spatial evolution in a repeated *s*-SNOM line-scan along the longitudinal (c_{R}) axis of a crystal with corresponding topography (panel e) as a function of temperature. The appearance

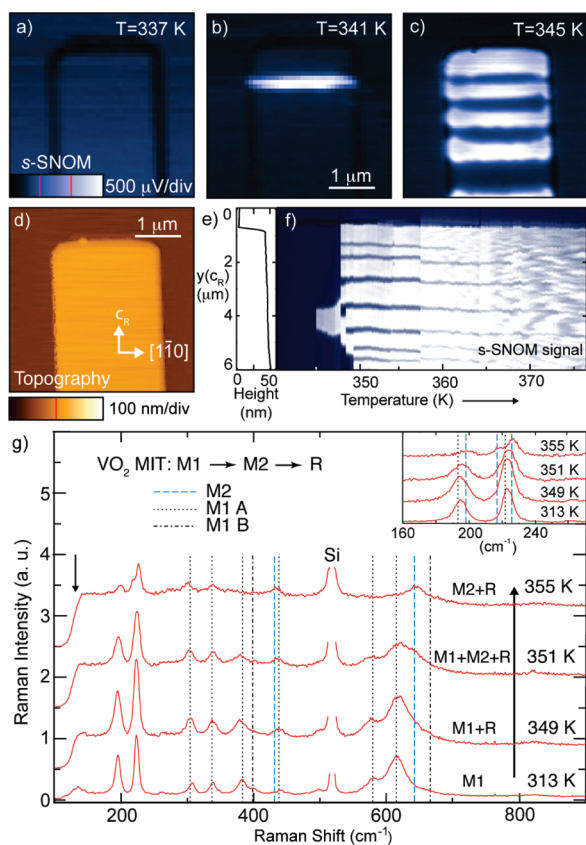


FIGURE 2. *s*-SNOM images (a–c) with corresponding topography (d) of a VO₂ crystal ($h = 35$ nm) initially in the M1 insulating phase (a), and its metallic/insulating domain formation (b,c) as the crystal is heated through the MIT. Corresponding longitudinal line scan tracing the spatial domain formation on a similar VO₂ crystal with sample heating (e,f). The phases of the insulating domains are identified by Raman measurements (g) finding M1 + M2 + R (351 K) and M2 + R (355 K) intermediate phase coexistence regimes.

of the first metallic domain in the scan region is followed by a splitting, rearrangement, and subsequent formation of the alternating domain pattern indicating the intermediate superheating and sudden release of stress energy. With the enhanced spatial resolution of ≈ 30 nm provided by *s*-SNOM, it can be seen that thin insulating domains persist up to $T > 375$ K. The increase in *s*-SNOM noise with increasing temperature is the result of tip/cantilever heating and related jitter in the force feedback.

In contrast to the sudden formation of metallic domains during the heating cycle, upon cooling the MIT is a gradual process with a continuous shrinking of the metallic domains (see Supporting Information). The final disappearance of the last metallic domains beyond *s*-SNOM sensitivity and resolution of width as small as 50 nm is observed at temperatures as low as $T = 330$ K indicating a pronounced hysteresis at the low temperature side of the MIT. Unfortunately, in IR *s*-SNOM measurements it is difficult to distinguish between the M1 and M2 phases which appear to have only small differences in their dielectric properties in the infrared.⁴⁴ However, comparison of Raman and high spatial resolution

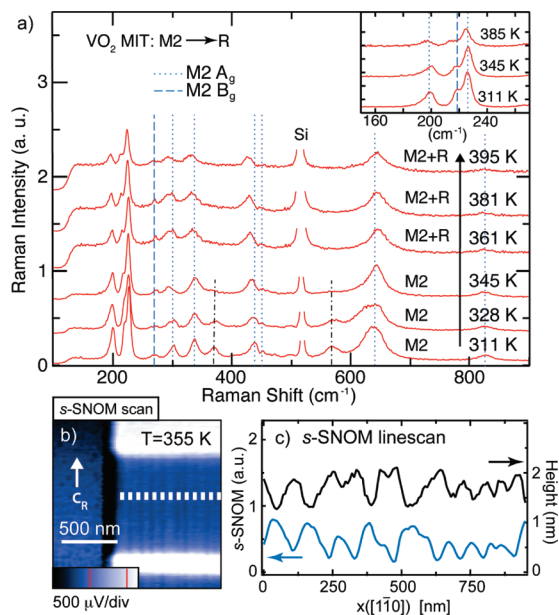


FIGURE 3. Sequence of Raman spectra on heating of a single VO₂ crystal initially in the M2 insulating phase at room temperature (a) with MIT proceeding via a M2 + R phase coexistence only. Periodic metallic domain formation (bright regions) and additional weaker subdomain contrast pattern in the M2 insulating state (b) due to twinning (see text for details). *s*-SNOM contrast correlated with ~ 1 nm topographic variations (c, line-scan along dashed line in b).

s-SNOM results indicates that the M1 \rightarrow M2 transition occurs at a stage of the MIT where between 70 and 85% of the crystal is in R phase.

Figure 3 shows Raman and *s*-SNOM results for crystals that are initially fully in the M2 phase at room temperature. On warming, the first emergence of R domains is observed near 360 K, that is, at temperatures higher than that found for crystals initially in the M1 phase at room temperature. As the temperature increases the periodic domain formation and their spatial evolution proceeds in a qualitatively similar fashion to the case above. However, as the Raman spectra indicate, the insulating phase in these crystals remains purely M2 throughout the entire transition and over the entire temperature range investigated with no trace of M1 appearing. With temperatures as high as 410 K, the purely metallic phase is found to be complete at temperatures higher (30 K) than in crystals originally in M1. Interestingly, at low temperatures before the appearance of the first metallic domains, two additional Raman modes at 362 and 568 cm^{-1} can be discerned that are not attributable to either the M1 or M2 phases and whose amplitude decreases with temperature. Measurements under controlled stress⁵⁰ indicate that these resonances are related to tensile stress and are an indication that the crystallite is near the M1/M2 phase boundary.

Only for crystals initially in the M2 phase, an additional weak *s*-SNOM contrast was observed in the insulating phase in the form of periodic striation parallel to c_R (Figure 3b). The contrast is only $\sim 3\%$ of the metal–insulator contrast. These

signal variations with a period of ~ 100 nm are correlated with slight variations in surface topography of ~ 1 nm (Figure 3c). This observation can be attributed to polysynthetic twinning of the M2 phase of the VO₂ crystals as shown recently by micro X-ray diffraction measurements of strained crystals.²⁶ The resulting birefringence can give rise to a polarization modulation of the tip-scattered signal and thus slight variations in the s-SNOM contrast. The s-SNOM/topographic striation is found to be independent of temperature while the crystal remains in the insulating phase with the signal variations disappearing upon conversion to the metallic phase. The modulation pattern reappears after cooling and the emergence of the M2 phase. No change in the characteristic M2 Raman spectral signature associated with this M2 subdomain patterning is found.

Discussion. From the results shown above and similar measurements of VO₂ crystals of different sizes and shapes, we conclude that crystals initially in the M1 phase at room temperature convert to the metallic phase via a sequence of (a) formation of periodic metallic domains followed by (b) the conversion of the M1 insulating domains into the M2 phase, and finally (c) the growth and convergence of the metallic domains into the fully metallic phase of the crystal, M1 \rightarrow M1 + R \rightarrow M2 + R \rightarrow R. Those crystals found initially in the M2 phase convert directly via the formation of periodic metallic domains and their gradual growth through heating into the fully metallic state, M2 \rightarrow M2 + R \rightarrow R.

While the actual three-dimensional stress field within these crystals is complicated and varying throughout the transition, the largest relative change in lattice constants between the three phases occurs along the c_R axis. Metallic stripes are always seen to form perpendicular to this axis even in wide crystals with small aspect ratios. We therefore consider a simple model to describe the phase/domain behavior which assumes the elastic energy to be governed primarily by the axial stress in the c_R direction σ with σ_{ave} representing a spatial average over the crystal. The source of this axial stress is the strain mismatch δ of the differing constituent phases of the crystal with the substrate. It is important to note, that while σ_{ave} may be close to zero due to the alternating compressive and tensile stress, the respective elastic energy of the for all domains is nonzero.

However, σ_{ave} has physical significance as it is proportional to the net stress applied to the crystal via the substrate. The observation that these stressed VO₂ crystals form domains as they move through the MIT indicates that minimization of the elastic energy of the substrate outweighs internal energy gain within the crystal due to the elastic energy, free energy density, and domain wall formation required to create a periodic set of domains (see Figure 4b). In the fully insulating or metallic state we assume that σ is nearly uniform along the crystal and equal to σ_{ave} . In the coexistence regime during the MIT, σ should vary along the c_R crystal axis as the structure alternates between insulating (more positive/compressive stress) and metallic (more nega-

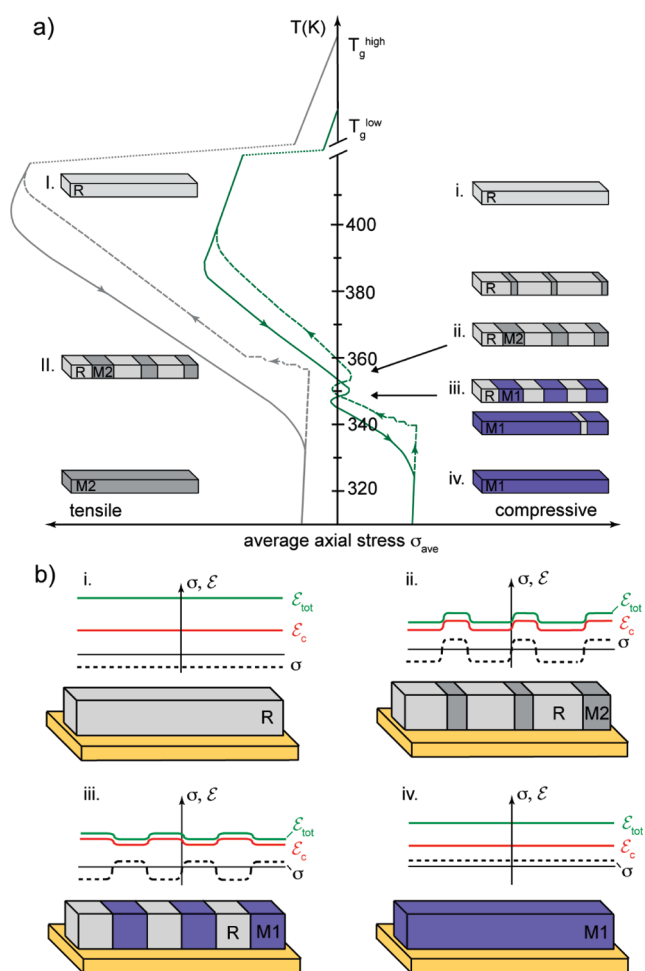


FIGURE 4. (a) Schematic of the MIT domain evolution of VO₂ crystals as a function of temperature and its relationship with the average external axial stress. Dashed/solid lines indicate heating/cooling curves, respectively. Relationship (b) between the domain configuration with stress σ within individual domains (dashed line), the associated elastic energy density of the crystal ϵ_c (solid red line), and the elastic energy of the crystal/substrate system ϵ_{tot} for a crystal stabilized in the M1 phase at room temperature at stages i–iv during the MIT.

tive/tensile stress) domains. This corresponds to a reduction of the average stress, and therefore the total elastic energy of the crystal/substrate system.

Figure 4a shows a graphical representation of the phase and domain evolution of the VO₂ crystal with temperature with the associated average axial stress σ_{ave} . The stress-temperature correlation shown in this figure takes into account the combined knowledge from measurements of the spatial evolution of domains provided by s-SNOM, the observation of phase composition yielded by Raman measurements, previous characterization of the crystallographic phases,^{9,29} and understanding of sample growth conditions. The solid (dashed) lines represent the behavior of σ_{ave} during cooling (heating).

As a result of the different thermal expansion coefficients ($\alpha_R > \alpha_S$) during the initial cooling after fusion of the crystal to the substrate, at temperatures slightly above the MIT the

crystal experiences tensile stress (Figure 4a, region i, I). This tensile stress may be approximated through estimation of the strain mismatch of the crystal in the R phase, $\delta_R \approx (\alpha_R - \alpha_{Si})(T - T_g)$. Here, T_g represents the temperature at which the crystal grows on the substrate.

For all crystals (both those in M1 and those in M2 at room temperatures), on cooling toward the transition σ_{ave} can be reduced most effectively by introducing thin M2 domains.⁴⁵ This is consistent with the observation that the insulating phase at higher temperatures is initially M2. An associated consequence of the tensile strain is that the first appearance of insulating domains occurs well above T_{MIT} ; indeed, we observe the appearance of insulating domains as high as ≈ 400 K. Upon further cooling, M2 domains grow continuously with decreasing temperature, thus reducing σ_{ave} further (Figure 4a, region ii, II).

For the crystals in the M1 phase at room temperature, on cooling to a temperature of ~ 350 K at which $\sim 25\%$ of the crystal is in the insulating phase the remaining insulating domains convert from the M2 to M1 phase within a 4–5 K temperature range. *s*-SNOM measurements indicate only a $\sim 4\%$ change in the volume fraction of the crystal occupied by the R phase within this temperature window over which the M2→M1 conversion occurs for typical crystals. This conversion of the insulating regions can be understood in terms of the continuous growth of the M2 domains with σ eventually becoming locally compressive. Compressive stress for the M1 phase is consistent with the previously reported compressive stress value of 0.4%.²³ With compressive stress the M1 phase with its shorter axial lattice constant and lower free energy becomes more favorable than the M2.

After the complete conversion of M2 to M1, further cooling results in the steady growth of the insulating domains until the fully insulating state is reached (Figure 4a, region iii). The persistence of R domains below the bulk transition temperature is consistent with compressive stress favoring the R phase with its shorter lattice constant. The compressive stress is also revealed by the fact that crystals are found to buckle when released from the substrate for transport devices with their ends fixed by evaporated electrodes.²³

Upon heating (dashed green line) these crystals exhibit the first emergence of R domains near the bulk transition temperature (Figure 2f, 340–350 K). The initial discrete appearance of almost micrometer-size R domains should result in a stepwise reduction of the average compressive stress as indicated. The formation of periodic R domains and their gradual widening may make the stress in the adjacent insulator tensile, promoting the conversion of the insulating domains from M1 to M2 at ~ 350 K (Figure 2g, 351, 355 K) with a hysteresis of ~ 5 K relative to the cooling case. This conversion is followed by the steady growth of the R domains (Figure 2f, 350–370 K) resulting finally in a fully metallic crystal under tensile stress. The hysteresis observed at the beginning and end of the MIT is asymmetric with a

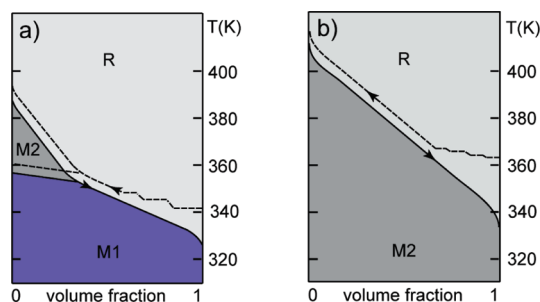


FIGURE 5. Associated temperature dependence of crystal volume fraction in the M1, M2, and R phases for a crystallite initially in the M1 at room-temperature (a). Corresponding diagram for crystals found in the M2 phase at room-temperature (b).

less than 5 K offset between disappearance and first reappearance of insulating M2 domains at higher temperature but a > 10 K between the discrete appearance of metallic domains on warming versus the gradual disappearance of metallic domains on cooling (see Supporting Information).

For a crystal found stabilized in M1 at room temperature, Figure 4b illustrates the relationship between the stress experienced by domains of different phase within a crystal with both the elastic energy density of the crystal ϵ_c and the elastic energy density of the crystal/substrate system ϵ_{tot} at various stages of the MIT. Here, upon cooling the formation of domains (i→ii) results in a release of the substrate stress and thus a reduction in ϵ_{tot} . Growth of the insulating domains eventually results in a conversion of insulating M2 domains to M1 to lower the stress applied by the substrate (ii→iii). Finally, further cooling leads to the formation of a fully insulating wire (iii→iv) under compressive stress as dictated by the substrate. Here again, the substrate related stress results in an overall increase in ϵ_{tot} .

Figure 5a shows the temperature dependence of the approximate volume fraction of the different phases during heating and cooling (dashed and solid lines, respectively), derived from analysis of the *s*-SNOM images and the Raman phase identification. While the details vary somewhat between different crystals the general behavior is reproducible. The corresponding volume fraction plot for the set of crystals in M2 at room temperature is shown in Figure 5b. For these crystals, the temperature at which the first M2 domains appear is higher compared to crystals stabilized in the M1 phase at room temperature. This suggests that a higher initial tensile stress differentiates these crystals from the M1 crystals. Such higher built in tensile stress for M2 at temperatures slightly above T_{MIT} with respect to their M1 counterparts could result from a higher growth/fusing temperature T_g . This would be consistent with the observation that upon warming R domains appear at temperatures 10–20 K higher than T_{MIT} (Figure 3a, up to 361 K). This furthermore fits with our observation that crystals grown further upstream (higher T_g) within the temperature gradient in the furnace tend to be in the M2 phase at room temperature. That the details of crystal growth may affect the phase of VO_2 at room tem-

perature underscores the importance of the role of stress in the MIT and is consistent with previous studies which have linked M2 stabilization to small system perturbations.^{9–11,46}

Our results offer a cautionary note for interpreting measurements of VO₂ samples in general and polycrystalline thin films in particular. In the latter nanoscale heterogeneities with crystallites of different sizes, individual local stress conditions, and random distribution of the crystallographic orientations obscure the intrinsic properties of the individual phases in macroscopic measurements. Indeed, a stochastic behavior in such films was observed,⁴⁷ and previous *s*-SNOM studies on polycrystalline films revealed a complex correlation between the MIT and, for example, film morphology, topography, and grain boundaries.^{20,21}

Our work identifies an even more complex combination of multiple nanoscale phase and domain heterogeneities than previously assumed²² even in small, perfect single crystals adhering to substrates or to each other, as a result of elastic effects. Not only do we see the expected mixture of metallic and insulating domains with new morphological details revealed by sensitive high resolution *s*-SNOM probing, but we also observe an unexpected pervasive presence of the M2 insulating phase and its competition with M1 within single crystals, an observation consistent with the known ready stabilization of M2 by doping and moderate stress.^{9–11} From these results, we conclude that M2 should be present over a certain temperature range around the MIT, at least transiently, in polycrystalline thin films, given the unavoidable local stress due to the MIT of individual crystallites, as well as most likely in bulk VO₂ samples. If this conclusion proves correct, the possibility of a transient M2 insulating phase involved in the MIT should be considered for samples with undefined crystallographic orientation. This consideration may apply not only for static measurements like the one performed here, but also for ultrafast measurements where the transition has been found to depend not only on photodoping but atomic motion of the unit cell as well.⁴⁹ We note that although Raman signatures of M2 were not recognized in earlier studies of thin films, their observation would have been difficult due to the obscuring presence of V₂O₅ Raman lines in that case.³⁸

Studying small single crystals offers the opportunity for a new methodical approach to the MIT in VO₂. In addition to their excellent homogeneous form and resistance to degradation, it is possible to apply a uniform and controlled stress after release from the substrate.^{23,24} The combination of nano-optical, ultrafast, and electrical measurements should then allow precise determination of the properties of each of the multiple individual homogeneous phases and their conversion by stress, and clarification of the possibly key role of the intermediate M2 phase^{8,14} as well as other aspects of the mechanism behind the MIT in this archetypal strongly correlated material.

In conclusion, our results underscore the general importance of understanding the implications of any inhomoge-

neous variation in the local stress distribution on the properties of complex systems with phase transitions with associated lattice changes in general and VO₂ in particular. The insight provided by the combination of different optical spectroscopies with *s*-SNOM highlights the potential of new nano-optical techniques to isolate and probe the intrinsic optical response of individual nanoscale domains desired for the characterization of the wide range of correlated electron systems.

Acknowledgment. This research was supported by the National Science Foundation under NSF CAREER Grant CHE 0748226 and DMR-0451788, the U.S. Department of Energy, Office of Basic Energy Sciences, Division of Materials Sciences and Engineering under Award DE-SC0002197, and by the Army Research Office under contract number 48385-PH. Support from the Nanotech User Facility (NTUF) at the University of Washington is greatly acknowledged as is support under a National Science Foundation Graduate Research Fellowship (A.C.J) and IGERT fellowship (S.B.). The authors further wish to thank Junqiao Wu and Jinbo Cao for valuable discussion.

Supporting Information Available. Discussion of cooling behavior and Figure 6. This material is available free of charge via the Internet at <http://pubs.acs.org>.

REFERENCES AND NOTES

- (1) Morin, F. J. *Phys. Rev. Lett.* **1959**, *3*, 34–36.
- (2) Mott, N. *Rev. Mod. Phys.* **1968**, *40*, 677–8.
- (3) Goodenough, J. B. *J. Solid State Chem.* **1971**, *3*, 490–500.
- (4) Zylbersztejn, A.; Mott, N. F. *Phys. Rev. B* **1975**, *11*, 4383–4395.
- (5) Paquet, D.; Leroux-Hugon, P. *Phys. Rev. B* **1980**, *22*, 5284–5301.
- (6) Wentzcovitch, R. M.; Schulz, W. W.; Allen, P. B. *Phys. Rev. Lett.* **1994**, *72*, 3389–3392.
- (7) Wentzcovitch, R. M.; Schulz, W. W.; Allen, P. B. *Phys. Rev. Lett.* **1994**, *73*, 3043.
- (8) Rice, T. M.; Launois, H.; Pouget, J. P. *Phys. Rev. Lett.* **1994**, *73*, 3042.
- (9) Marezio, M.; McWhan, D. B.; Remeika, J. P.; Dernier, P. D. *Phys. Rev. B* **1972**, *5*, 2541–2551.
- (10) Pouget, J. P.; Launois, H.; D’Haenens, J. P.; Merenda, P.; Rice, T. M. *Phys. Rev. Lett.* **1975**, *35*, 873–875.
- (11) Sohn, J. I.; Joo, H. J.; Ahn, D.; Lee, H. H.; Porter, A. E.; Kim, K.; Kang, D. J.; Welland, M. E. *Nano Lett.* **2009**, *9*, 3392–3397.
- (12) Chamberland, B. *J. Solid State Chem.* **1973**, *7*, 377–384.
- (13) Galy, J. J. *Solid State Chem.* **1999**, *148*, 224–228.
- (14) Eyert, V. *Ann. Phys. (Leipzig)* **2002**, *11*, 650–702.
- (15) Zhang, S.; Chou, J. Y.; Lahun, L. J. *Nano Lett.* **2009**, *9*, 4527–4532.
- (16) Maurer, D.; Leue, A. *Mater. Sci. Eng. A* **2004**, *370*, 440–443.
- (17) Chain, E. E. *Appl. Opt.* **1991**, *30*, 2782–2787.
- (18) Choi, H. S.; Ahn, J. S.; Jung, J. H.; Noh, T. W.; Kim, D. H. *Phys. Rev. B* **1996**, *54*, 4621–4628.
- (19) Chang, Y.; Koo, C.; Yang, J.; Kim, Y.; Kim, D.; Lee, J.; Noh, T.; Kim, H.-T.; Chae, B. *Thin Solid Films* **2005**, *486*, 46–49.
- (20) Qazilbash, M.; Brehm, M.; Chae, B.-G.; Ho, P.-C.; Andreev, G.; Kim, B.-J.; Yun, S.; Balatsky, A.; Maple, M.; Keilmann, F.; Kim, H.-T.; Basov, D. *Science* **2007**, *318*, 1750.
- (21) Frenzel, A.; Qazilbash, M. M.; Brehm, M.; Chae, B.-G.; Kim, B.-J.; Kim, H.-T.; Balatsky, A. V.; Keilmann, F.; Basov, D. N. *Phys. Rev. B* **2009**, *80*, 115115.
- (22) Wu, J.; Gu, Q.; Guiton, B.; deLeon, N.; Ouyang, L.; Park, H. *Nano Lett.* **2006**, *6*, 2313–2317.
- (23) Wei, J.; Wang, Z.; Chen, W.; Cobden, D. H. *Nat. Nanotechnol.* **2009**, *4*, 420–424.

- (24) Cao, J.; Ertekin, E.; Srinivasan, V.; Fan, W.; Huang, S.; Zheng, H.; Yim, L. J. W.; Khanal, R. D.; Ogletree, F. D.; Grossman, C. J.; Wu, J. *Nat. Nanotechnol.* **2009**, [Online early release].
- (25) Hillenbrand, R.; Keilmann, F. *Phil. Trans. R. Soc. London, Ser. A* **2004**, *362*, 787–805.
- (26) Cao, J.; Fan, W.; Gu, Y.; Chen, L.; Ogletree, D.; Chen, K.; Tamura, N.; Kunz, M.; Barrett, C.; Seidel, J.; Saiz, E.; Wu, J. Submitted for publication.
- (27) The dimerization of the A sublattice for the M2 and both the A and B sublattices for the M1 is responsible for the quadrupling and doubling of the M2 and M1 unit cells respectively.
- (28) McWhan, D. B.; Marezio, M.; Remeika, J. P.; Dernier, P. D. *Phys. Rev. B* **1974**, *10*, 490–495.
- (29) Kucharczyk, D.; Niklewski, T. J. *Appl. Crystallogr.* **1979**, *12*, 370–373.
- (30) Guiton, B.; Gu, Q.; Prieto, A.; Gudixsen, M.; Park, H. *J. Am. Chem. Soc.* **2005**, *127*, 498–499.
- (31) Sridhar, N.; Rickman, J.; Srolovitz, D. *Acta Mater.* **1996**, *44*, 4097–4113.
- (32) Rang, M.; Jones, A.; Zhou, F.; Li, Z.-Y.; Wiley, B.; Xia, Y.; Raschke, M. *Nano Lett.* **2008**, *8*, 3357–3363.
- (33) Barker, A. S.; Verleur, H. W.; Guggenheim, H. J. *Phys. Rev. Lett.* **1966**, *17*, 1286–1289.
- (34) Qazilbash, M. M.; Burch, K. S.; Whisler, D.; Shrekenhamer, D.; Chae, B. G.; Kim, H. T.; Basov, D. N. *Phys. Rev. B* **2006**, *74*, 205118.
- (35) Gozhenko, V.; Grechko, L.; Whites, K. *Phys. Rev. B* **2003**, *68*, 125422.
- (36) Raschke, M. B.; Lienau, C. *Appl. Phys. Lett.* **2003**, *83*, 5089–5091.
- (37) Srivastava, R.; Chase, L. L. *Phys. Rev. Lett.* **1971**, *27*, 727–730.
- (38) Petrov, G. I.; Yakovlev, V. V.; Squier, J. *Appl. Phys. Lett.* **2002**, *81*, 1023–1025.
- (39) Schilbe, P. *Physica B* **2002**, *316*, 600–317.
- (40) Marini, C.; Arcangeletti, E.; Di Castro, D.; Baldassare, L.; Perucchi, A.; Lupi, S.; Malavasi, L.; Boeri, L.; Pomjakushina, E.; Conder, K.; Postorino, P. *Phys. Rev. B* **2008**, *77*, 235111.
- (41) Chou, J. Y.; Lensch-Falk, J. L.; Hemesath, E. R.; Lauhon, L. J. *J. Appl. Phys.* **2009**, *105*, No. 034310.
- (42) While the characteristic Raman peaks observed here agree well with previous measurements,⁴⁰ the exact mechanism behind the metastable stabilization of these freestanding structures that likely involves the localized heating/strain associated with the laser focus is difficult to characterize.
- (43) Kuzmany, H. *Solid State Spectroscopy*; Springer: New York, 1998.
- (44) Complementary tip-enhanced Raman scattering (TERS) imaging suffered under the low phonon Raman cross sections of VO₂.⁴⁸
- (45) A fully rigorous treatment of the MIT of substrate bound crystals must account for several energy contributions and the interplay of strain inhomogeneities, domain wall energy, interfacial effects, and the free energy densities of the individual phases.
- (46) Pouget, J. P.; Launois, H.; Rice, T. M.; Dernier, P.; Gossard, A.; Villeneuve, G.; Hagenmuller, P. *Phys. Rev. B* **1974**, *10*, 1801–1815.
- (47) Sharoni, A.; Ramirez, J. G.; Schuller, I. K. *Phys. Rev. Lett.* **2008**, *101*, No. 026404.
- (48) Berweger, S.; Raschke, M. B. *Anal. Bioanal. Chem.* **2010**, *396*, 115.
- (49) Cavalleri, A.; Rini, M.; Schoenlein, R. W. *J. Phys. Soc. Jpn.* **2006**, *75*, No. 011004.
- (50) Jones, A.; Berweger, S.; Raschke, M. B.; Cao, J.; Wu, J. Private Communication.